Coordination behaviour of 1-(4,2':6',4''-terpyridin-4'-yl)ferrocene and 1-(3,2':6',3''-terpyridin-4'-yl)ferrocene: predictable and unpredictable assembly algorithms

Y. Maximilian Klein,[A] *A. Prescimone,*[A] *E. C. Constable,*[A] *and C. E. Housecroft*[A]*

[A]Department of Chemistry, University of Basel, Spitalstrasse 51, CH4056 Basel, Switzerland

email: catherine.housecroft@unibas.ch

ABSTRACT

The reaction of 1-(4,2':6',4''-terpyridin-4'-yl)ferrocene (**2**) with ZnI_2 leads to $[\{ZnI_2(\mathbf{2})\}_4 \cdot 1.4MeOH \cdot 0.8H_2O]$ which contains a discrete [4+4] metallocycle. Crystal growth experiments demonstrate that reactions of **2** with $Zn(OAc)_2$ or $CuCl_2$ result in the formation of single- or double-stranded 1D-polymer chains, respectively, the latter facilitated by the formation of $\{Cu_2Cl_4\}$ dinuclear nodes. Whilst both **2** and its isomer 1-(3,2':6',3''-terpyridin-4'-yl)ferrocene (**3**) present V-shaped donor sets, rotation about interannular bonds in **3** generates flexible vectorial properties associated with limiting convergent and divergent orientations of the nitrogen donors. The synthesis and characterization of **3** are described as are reactions of **3** with $ZnCl_2$ or $ZnBr_2$ which lead, respectively, to a metallosquare in $[\{ZnCl_2(\mathbf{3})\}_4 \cdot 3CHCl_3 \cdot 3MeOH]$ or a helical polymer in $[\{ZnBr_2(\mathbf{3})\} \cdot MeOH]_n$. The tight pitch of the helix in the latter (8.7879(9) Å) is controlled by a combination of the orientations of the *N,N*''-donor sets in **3**, and intra-chain π-stacking interactions involving ferrocenyl and pyridine units.

Dedication: We dedicate this work to our good friend Len Lindoy on the occasion of his 80th birthday – Len, you have been an inspiration and colleague to two of the authors for over 30 years.

Introduction

N-Heterocyclic ligands containing ferrocenyl units can be easily modified to incorporate different functionalities and to imbue tunable properties to their metal complexes.[1] Materials incorporating

ferrocene-building blocks can show interesting magnetic and electrochemical properties, in particular in multimetallic polymers.[2,3] A recent example from Kraatz and coworkers demonstrates that using a ferrocene substituent in an artificial peptide produces a versatile, redox-responsive material.[4] The incorporation of ferrocenyl-units also allows the development of promising properties for applications including photoinduced electron transfer,[5] electrochemical sensing[6] and enhanced stability and reactivity in palladium based catalysts for cross-coupling reactions.[7,8]

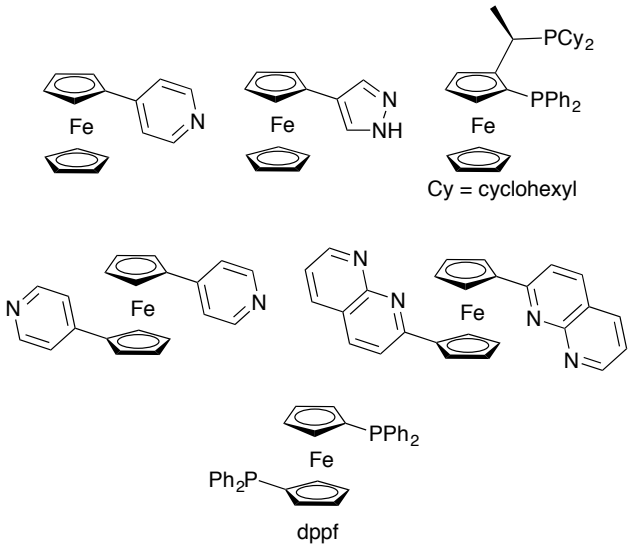

Scheme 1. Examples of mono- and disubstituted ferrocenyl ligands used for the assembly of discrete complexes and coordination polymers.

Some representative ferrocenyl-containing ligands are shown in Scheme 1. Functionalization of one cyclopentadienyl ring typically leads to ligands suited to the formation of discrete complexes,[9,10] and the chiral ligand at the top-right of Scheme 1 is of note for its use in giving enhanced stability and crystallization behaviour in palladium complexes utilized in cross-coupling reactions.[8] Functionalization of both cyclopentadienyl rings with donor groups produces potential linkers in multinuclear assemblies including metallocycles and coordination polymers.[11] On the one hand, the conformational flexibility of the ferrocenyl unit through independent rotation of the Cp rings about the iron atom "ball-bearing" endows 1,1'-substituted ferrocenes with a degree of freedom facilitating the assembly of diverse architectures.[12,13,14] However, this rotational freedom, whilst permitting access to a broad conformational space also reduces the preorganization of the assembly process, making structural engineering design less

predictable. 1,1'-Bis(phosphino)ferrocene ligands such as dppf (Scheme 1) are widely investigated and form both discrete complexes[15] and coordination polymers[16] with a range of metal ions. An alternative approach is the design of *N*-heterocyclic ligands suited to coordination polymer assembly by covalently attaching one or more divergent multinucleating donor sets to the ferrocenyl core. We have demonstrated that 1,1'-(4,2':6',4''-terpyridin-4'-yl)ferrocene (**1**, Scheme 2) reacts with $ZnCl_2$ to give an unusual double-stranded 1D-coordination polymer, the assembly of which is directed by a combination of a *cisoid*-ferrocene moiety and π-π interactions between 4,2':6',4''-terpyridine (4,2':6',4'-tpy) domains.[17] This contrasts with related double-, triple- or quadruple-stranded coordination polymers which have their origins in multinuclear metal nodes[18,19,20] rather than in the ligand-linker. Tian and coworkers recently reported reactions of 1-(4,2':6',4''-terpyridin-4'-yl)ferrocene (**2**, Scheme 2) with zinc(II) salts.[21] Ligand **2** reacts with $ZnCl_2$ and $ZnBr_2$ to give discrete metallohexacycles similar to those obtained with other 4'-substituted 4,2':6',4'-tpy ligands.[22] 1D-coordination polymers result when **2** is treated with ZnI_2, $Zn(NCS)_2$ and $Zn(OAc)_2$. We now report the synthesis and coordination behaviour of 1-(3,2':6',3''-terpyridin-4'-yl)ferrocene (**3**, Scheme 2) with $ZnCl_2$ and $ZnBr_2$, and also demonstrate competitive assembly pathways to different structure types using ligands **2** and **3**.

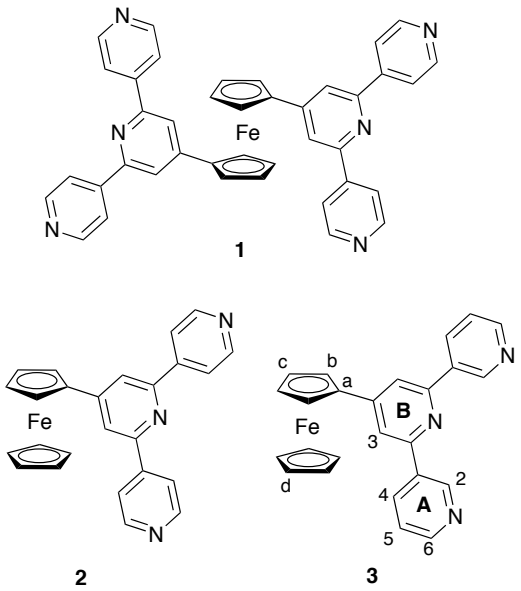

Scheme 2. Structures of ligands **1**–**3**, and numbering scheme of **3** used for NMR spectroscopic assignments.

Experimental Section

General

^{1}H and ^{13}C NMR spectra were recorded on a Bruker Avance III-500 spectrometer with chemical shifts referenced to residual solvent peaks, δ(TMS) = 0 ppm. Electrospray ionization (ESI) mass spectra were recorded on a Bruker esquire 3000^{plus} mass spectrometer. Ligand **2** was prepared as previously reported.[21]

Compound 3

Ferrocenecarboxaldehyde (1.0 g, 4.67 mmol) was dissolved in EtOH (150 mL). 3-Acetylpyridine (1.24 g, 10.3 mmol) and KOH (0.66 g, 11.7 mmol) were added to the solution and a change from red to dark red was observed. Aqueous NH_3 (32%, 18.0 mL) was slowly added to the reaction mixture which was then stirred at room temperature for ~15 h. The solid that formed was collected by filtration, washed with EtOH (3 × 20 mL) and H_2O (3 × 20 mL) and dried in vacuo. Compound **3** was isolated as a red powder (0.83 g, 1.99 mmol, 43%). Dec. > 210 °C. ^{1}H NMR (500 MHz, CD_3OD) δ / ppm 9.38 (d, J = 2.2 Hz, 2H, H^{A2}), 8.68 (m, 2H, H^{A4}), 8.63 (dd, J = 4.9, 1.6 Hz, 2H, H^{A6}), 8.05 (s, 2H, H^{B3}), 7.62 (dd, J = 8.0, 4.9 Hz, 2H, H^{A5}), 5.15 (m, 2H, H^{b}), 4.55 (m, 2H, H^{c}), 4.11 (s, 4H, H^{d}). $^{13}C\{^{1}H\}$ NMR (126 MHz, CD_3OD) δ / ppm 155.7 (C^{B2}), 153.7 (C^{B4}), 150.3 (C^{A6}), 148.8 (C^{A2}), 136.8 (C^{A3}), 136.6 (C^{A4}), 125.4 (C^{A5}), 117.8 (C^{B3}), 81.82 (C^{a}), 71.8 (C^{c}), 71.1 (C^{d}), 68.5 (C^{b}). ESI-MS m/z 417.9 $[M+H]^+$ (calc. 418.1). Found C 69.83, H 4.89, N 9.73; required for $C_{25}H_{19}FeN_3 \cdot {}^{1}/_{2}H_2O$ C 70.44, H 4.73, N 9.86.

$[\{ZnI_2(2)\}_4 \cdot 1.4MeOH \cdot 0.8H_2O]$

A MeOH (8 mL) solution of ZnI_2 (6.38 mg, 0.02 mmol) was layered over a $CHCl_3$ (5 mL) solution of **2** (8.35 mg, 0.02 mmol) and the crystallization tube was left to stand at room temperature. Red crystals of $[\{ZnI_2(\mathbf{2})\}_4 \cdot 1.4MeOH \cdot 0.8H_2O]$ (1.7 mg, 0.0006 mmol, 12% based on Zn) were obtained after 1-2 weeks.

$[\{Zn(OAc)_2(2)\} \cdot MeOH \cdot H_2O]_n$

A MeOH (8 mL) solution of $Zn(OAc)_2 \cdot 2H_2O$ (4.39 mg, 0.02 mmol) was layered over a $CHCl_3$ (5 mL) solution of **2** (8.35 mg, 0.02 mmol) and the crystallization tube was left to stand at room temperature. Red crystals of $[\{Zn(OAc)_2(\mathbf{2})\}_n \cdot MeOH \cdot H_2O]_n$ (2.7 mg, 0.002 mmol, 10% based on Zn) were obtained after 1-2 weeks.

$[\{ZnCl_2(3)\}_4 \cdot 2CHCl_3]$

A MeOH (8 mL) solution of $ZnCl_2$ (2.73 mg, 0.02 mmol) was layered over a $CHCl_3$ (5 mL) solution of **3** (8.35 mg, 0.02 mmol) and the crystallization tube was left at room temperature. A few red crystals of $[\{ZnCl_2(\mathbf{3})\}_4 \cdot 2CHCl_3]$ were obtained after 1-2 weeks.

$[\{ZnBr_2(3)\} \cdot MeOH]_n$

A MeOH (8 mL) solution of $ZnBr_2$ (4.50 mg, 0.02 mmol) was layered over a $CHCl_3$ (5 mL) solution of **3** (8.35 mg, 0.02 mmol) and the crystallization tube was left to stand at room temperature. Red crystals of $[\{ZnBr_2(\mathbf{3})\}_n \cdot 1MeOH]_n$ (2.8 mg, 0.004 mmol, 20% based on Zn) were obtained after 1-2 weeks.

$[\{Cu_2Cl_4(2)_2(MeOH)\} \cdot 2.25MeOH \cdot H_2O \cdot CHCl_3]_n$

A MeOH (8 mL) solution of $CuCl_2$ (4.03 mg, 0.03 mmol) was layered over a $CHCl_3$ (5 mL) solution of **2** (12.5 mg, 0.03 mmol) and the crystallization tube was left to stand at room temperature. Red crystals of $[\{Cu_2Cl_4(\mathbf{2})_2(MeOH)\} \cdot 2.25MeOH \cdot H_2O \cdot CHCl_3]_n$ (3.7 mg, 0.003 mmol, 20% based on Cu) were obtained after 1-2 weeks.

Crystallography

Single crystal data were collected on a Bruker APEX-II diffractometer; data reduction, solution and refinement used APEX2, SuperFlip and CRYSTALS respectively.[23,24,25] Structure analysis used Mercury v. 3.6.[26,27] Crystallographic data are given in Table 1. For $[\{Cu_2Cl_4(\mathbf{2})_2(MeOH)\} \cdot 2.25MeOH \cdot H_2O \cdot CHCl_3]_n$, the SQUEEZE[28] procedure had to be used to treat part of the solvent region; the removed electron density equated to an additional H_2O molecule and a $CHCl_3$ molecule. The formulae, molecular mass and density were adjusted accordingly. In $[\{ZnCl_2(\mathbf{3})\}_4 \cdot 3CHCl_3 \cdot 3MeOH]$, two $CHCl_3$ molecules were modelled and then SQUEEZE[28] was used to treat the remaining part of the solvent region; the electron density that was removed equated to one extra $CHCl_3$ and three MeOH molecules. All the crystals of this compound were weakly diffracting at high angles; although a sufficient number of reflections were collected, a number did not pass the $I/2\sigma$ cutoff threshold and hence the data-to-parameter ratio is less than 10.

Table 1. Crystallographic data

Compound	**3**	[{ZnI_2(**2**)}$_4$·1.4MeOH ·0.8H_2O]	[{$Zn(OAc)_2$(**2**)} ·MeOH·H_2O]$_n$
Formula	$C_{25}H_{19}FeN_3$	$C_{101.40}H_{83.20}Fe_4I_8N_{12}O_{2.20}Zn_4$	$C_{59}H_{56}Fe_2N_6O_{10}Zn_2$
Formula weight	417.29	3005.20	1251.58
Crystal colour and habit	Orange plate	Red block	Red plate
Crystal system	Orthorhombic	Triclinic	Orthorhombic
Space group	$P2_12_12_1$	P–1	*Pbca*
a, b, c / Å	9.9004(5), 11.3629(6), 16.9105(9)	11.4704(10), 11.7733(10), 19.2202(17)	24.3420(15), 16.0495(10), 28.2141(17)
α, β, γ / °	90 90 90	90.351(4) 102.329(4) 91.929(4)	90 90 90
U / Å^3	1902.38(17)	2534.1(4)	11022.6(12)
D_c / Mg m^{-3}	1.457	1.969	1.508
Z	4	1	8
μ(Mo-$K\alpha$) / mm^{-1}	6.472	25.046	5.661
T / K	123	123	123
Refln. collected (R_{int})	7433 (0.036)	33089 (0.037)	73603 (0.054)
Unique refln.	3204	9131	10050
Refln. for refinement	2710	7691	8760
Parameters	263	589	712
Threshold	2σ	2σ	2σ
*R*1 (*R*1 all data)	0.0313 (0.0389)	0.0360 (0.0445)	0.0418 (0.0507)
*wR*2 (*wR*2 all data)	0.0685 (0.0741)	0.0851 (0.0899)	0.0906 (0.0939)
Goodness of fit	0.8994	0.9080	0.9044
CCDC deposition	1504341	1504338	1504343

Compound	[{Cu_2Cl_4(**2**)$_2$(MeOH)} ·2.25MeOH·H_2O·$CHCl_3$]$_n$	[{$ZnCl_2$(**3**)}$_4$·3$CHCl_3$·3MeOH]	[{$ZnBr_2$(**3**)}·MeOH]$_n$
Formula	$C_{54.25}H_{54}Cl_7Cu_2Fe_2N_6O_{4.25}$	$C_{102}H_{78}Cl_{14}Fe_4N_{12}Zn_4$	$C_{26}H_{23}Br_2FeN_3OZn$
Formula weight	1345.02	2668.57	674.52
Crystal colour and habit	Red plate	Red block	Red block
Crystal system	Monoclinic	Orthorhombic	Triclinic
Space group	$P2_1/n$	*Pccn*	P–1
a, b, c / Å	16.1181(12), 24.7209(18), 16.1565(11)	25.0374(9), 19.6115(7), 23.4639(9)	8.7879(7), 17.1107(14), 18.0340(14)
α, β, γ / °	90 112.267(4) 90	90 90 90	73.010(3) 80.594(3) 82.192(3)
U / Å^3	5957.5(8)	11521.3(7)	2547.3(4)
D_c / Mg m^{-3}	1.50	1.54	1.759
Z	4	4	4
μ(Mo-$K\alpha$) / mm^{-1}	7.913	8.882	9.589
T / K	123	123	123
Refln. collected (R_{int})	38865 (0.056)	76606 (0.182)	33199 (0.037)
Unique refln.	10865	10807	9306
Refln. for refinement	7219	5214	9066
Parameters	649	613	619
Threshold	2σ	2σ	2σ
*R*1 (*R*1 all data)	0.0565 (0.0863)	0.0934 (0.1562)	0.0469 (0.0477)
*wR*2 (*wR*2 all data)	0.1439 (0.1750)	0.2478 (0.3154)	0 .1123 (0.1125)
Goodness of fit	0.9640	1.0169	0.8948
CCDC deposition	1504340	1504342	1504339

Results and discussion

Synthesis and characterization of compound 3

The synthesis of compound **2** (Scheme 2) [18] has previously been reported. Although compound **3** (Scheme 2) has previously been prepared in two steps via the isolated 1,5-bis(3-pyridyl)-3-ferrocenyl-pentane-1,5-dione,[29] we find the one-pot method of Wang and Hanan[19] more convenient. Ferrocenecarboxaldehyde was reacted with two equivalents of 3-acetylpyridine under basic conditions followed by treatment with aqueous NH_3; **3** was isolated in 43% yield. The electrospray mass spectrum of **3** shows a base peak at *m/z* 417.9 corresponding to $[M+H]^+$. The ^1H (Fig. 1) and ^{13}C NMR spectra of a CD_3OD solution of **3** were assigned using COSY, NOESY, HMQC and HMBC methods; literature spectroscopic data for a $CDCl_3$ solution of **3** comprise unassigned signals.[29] The signal for H^{B3} (see Scheme 2) appears as a singlet at δ 8.05 ppm. In the NOESY spectrum, cross peaks between the signals for H^{B3} and H^{A2}, H^{A4} and H^{b} were observed. The unsubstituted Cp ring gave rise to a singlet at δ 4.11 ppm, and multiplets at δ 5.15 and 4.55 ppm were assigned to the functionalized Cp ring. The ^{13}C NMR resonance for quaternary C^{B4} could not be confirmed from the HMBC spectrum, but the signal assigned at δ 153.7 ppm is consistent with that in 1-(pyridin-4'-yl)ferrocene.[30]

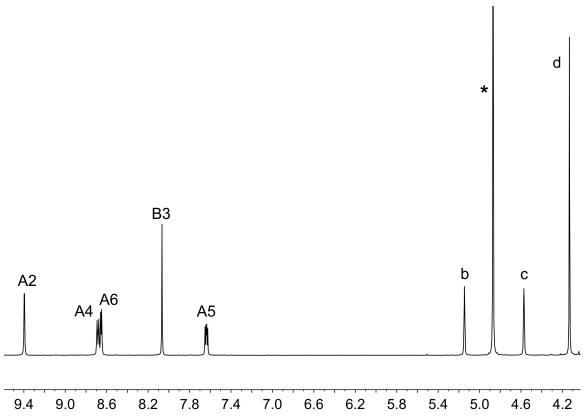

Fig. 1. 500 MHz ^1H NMR spectrum (CD_3OD) of compound **3**. * = Residual CD_3OH. See Scheme 2 for atom labels.

Single crystals of **3** were grown by slow evaporation of a $CHCl_3$ solution. Compound **3** crystallizes in the orthorhombic $P2_12_12_1$ space group, which is one of the 65 Sohnke space groups; the Flack parameter is 0.014. The structure of **3** is shown in Fig. 2a. The view in Fig. 2b reveals the chiral conformation adopted by the molecule in the lattice as a result of the restricted rotation about the C8–C16 bond (an example of

atropisomerism); the torsion angle C7–C8–C16–C17 is –28.8(4)°. The ferrocenyl unit has an eclipsed conformation, as is also observed in the solid-state structure of **2**.[21] In contrast to the adoption of a single atropisomer of **3** in the $P2_12_12_1$ space group, we note that **2** crystallizes in the centrosymmetric space group *P*–1.[21] In **3**, the pyridine rings containing N1 and N2 are approximately coplanar (angle between ring planes = 1.9°), whereas the ring with N3 is twisted through 35.0° with respect to the central pyridine ring. Close CH...N contacts (rather than π-stacking interactions) play an important role in the packing of molecules of **3**.

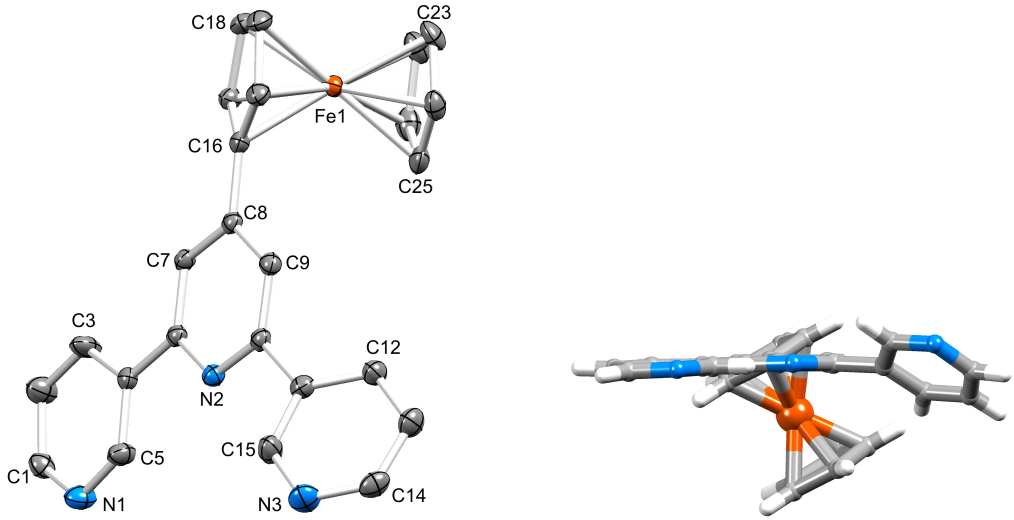

(a) (b)

Fig. 2. (a) Structure of compound **3**; H atoms omitted for clarity and ellipsoids plotted at 40% probability level. Important bond distances: C8 –C16 = 1.468(4), C1–N1 = 1.328(4), C5–N1 = 1.337(4), C6–N2 = 1.349(4), C10–N2 = 1.348(4), C14–N3 = 1.329(4), C15–N3 = 1.342(4) Å. (b) The chiral conformation adopted by **3** in the lattice.

Coordination polymer *versus* metallomacrocycle assembly with ligand 2

Typically, 4,2':6',4''-terpyridines coordinate only through the outer nitrogen atoms and are classed as divergent, V-shaped linkers.[22,31] During the course of our investigations of the coordination chemistry of the ferrocenyl-functionalized 4,2':6',4''- and 3,2':6',3''-terpyridines shown in Scheme 2, Tian and coworkers reported that **2** reacts with $ZnCl_2$ and $ZnBr_2$ to give the discrete metallohexacycles

[{$ZnCl_2$(**2**)}$_6$·6H_2O ·6$CHCl_3$] and [{$ZnBr_2$(**2**)}$_6$·6H_2O ·6$CHCl_3$].[21] Our own observations are consistent with these results.[32] Tian and coworkers also found that the 1D-coordination polymer [{ZnI_2(**2**)}·2$CHCl_3$]$_n$ forms over a period of days when a MeOH/$ZnCl_2$ solution is layered over a $CHCl_3$/**2** solution at room temperature.[21] In contrast, crystal growth under analogous conditions led, in our hands, to the discrete metallomacrocylic coordination compound [{ZnI_2(**2**)}$_4$·1.4MeOH·0.8H_2O]. This crystallizes in the triclinic space group *P*–1 with half of the centrosymmetric [4+4] metallocycle in the asymmetric unit. Fig. 2 shows the structure of the {ZnI_2(**2**)}$_4$ metallosquare. Each of the independent ferrocenyl units adopts an eclipsed conformation. The Cp_2Fe-unit containing Fe1 is twisted with respect to the 4,2':6',4''-tpy to which it is attached (angle between planes of rings containing N2 and C11 = 30.7°), consistent with minimizing close H...H interactions. In contrast, the Cp_2Fe unit with Fe2 exhibits a smaller twist (angle between planes of rings containing N5 and C36 = 8.1°), and this is related to the π-stacking interactions discussed below. Each Zn atom is tetrahedrally coordinated and the bond lengths and angles are unexceptional (Fig. 2 caption, and N–Zn–I bond angles are in the range 106.02(12) to 113.58(11)°). One 4,2':6',4''-tpy domain is slightly twisted with angles between the planes of the rings with N1/N2 and N2/N3 being 10.7 and 19.1°. The 4,2':6',4''-tpy unit containing atoms N4, N5 and N6 is close to planar (angles between planes of adjacent pyridine rings = 6.1 and 6.5°). The planarity is associated with intermolecular face-to-face π-stacking interactions (Fig. 3a) between pyridine rings containing N5/N6 and N5^{ii}/N6^{ii} (symmetry code ii = 1–*x*, –*y*, 1–*z*); the stacked heterocyclic rings are in an optimal offset orientation with an interplane separation of 3.37 Å and intercentroid distance of 3.73 Å. The tpy–tpy interaction is augmented by a centrosymmetric embrace of adjacent metallosquares (Fig. 3b) involving π-stacking interactions between the pyridine rings containing N4/N5 and one Cp ring of the ferrocene unit containing Fe2^{iii} (symmetry code iii = –*x*, –*y*, 1–*z*). The distance from the plane through the two pyridine rings to the centroid of the Cp ring with C45^{iii} is 3.30 Å, and $Cp_{centroid}$ to $pyridine_{centroid}$ separations are 3.69 and 4.20 Å.

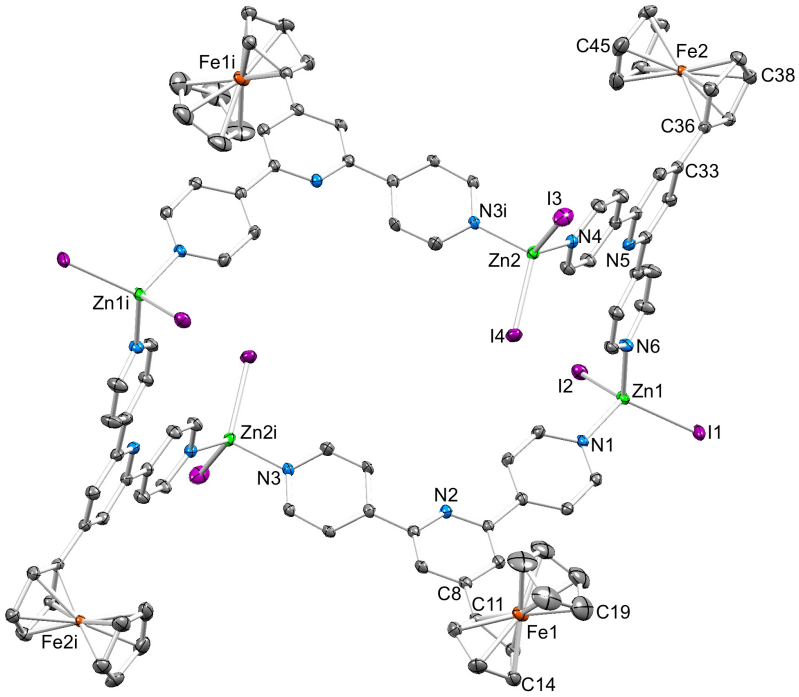

Fig. 2. Structure of the $\{ZnI_2(\mathbf{2})\}_4$ metallosquare in $[\{ZnI_2(\mathbf{2})\}_4 \cdot 1.4MeOH \cdot 0.8H_2O]$; H atoms omitted for clarity and ellipsoids plotted at 40% probability level. Symmetry code i = *–x*, *–y*, *–z*. Selected bond lengths and angles: Zn1–I1 = 2.5318(7), Zn1–I2 = 2.5455(8), Zn1–N1 = 2.043(4), Zn1–N6 = 2.056(4), Zn2–I3 = 2.5456(7), Zn2–I4= 2.5458(7), Zn2–N3i = 2.081(4), Zn2–N4 = 2.039(4) Å; I1–Zn1–I2 = 117.46(3), I3–Zn2–I4 = 115.08(3), N1–Zn1–N6 = 102.00(16), N3–Zn2–N4 = 99.64(15)°.

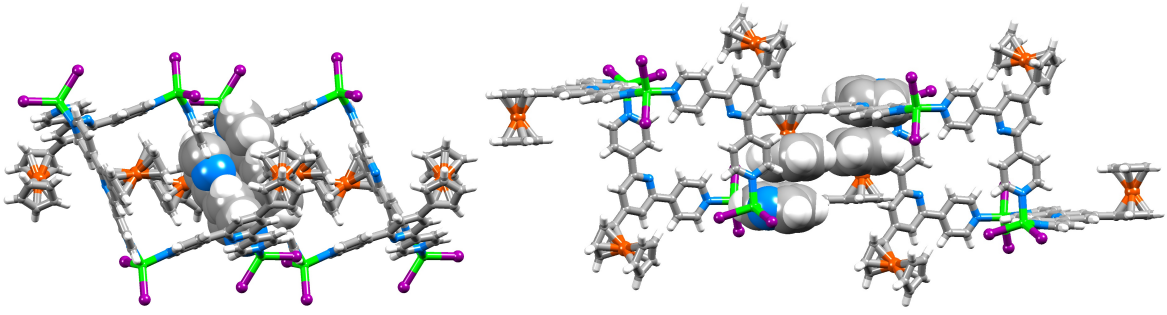

(a) (b)

Fig. 3. (a) Face-to-face π-stacking of 4,2':6',4''-tpy units between $\{ZnI_2(\mathbf{2})\}_4$ molecules; the structure is viewed down the crystallographic *c*-axis. (b) Centrosymmetric intermolecular embrace supported by Cp–pyridine π-stacking.

In an earlier investigation of molecular and polymer assemblies involving 4'-(2',3',4',5',6'-pentafluorobiphenyl-4-yl)-4,2':6',4''-terpyridine and zinc(II) halides, we observed competitive formation of a 1D-coordiantion polymer and a metallosquare in the same crystallization tube.[33] However, in the current investigation, powder diffraction data are consistent with [{ZnI_2(**2**)}$_4$·1.4MeOH·0.8H_2O] being representative of the bulk material obtained from the reaction of ZnI_2 and **2.** Figures S1 and S2 in the supporting material compare the powder diffraction patterns of the bulk sample obtained from the reaction of ZnI_2 and **2** with those predicted from the single crystal structure of [{ZnI_2(**2**)}$_4$·1.4MeOH ·0.8H_2O] (good agreement) and [{ZnI_2(**2**)}·2$CHCl_3$]$_n$ (CSD[34] recode TUNKEU[21], poor agreement). This result once again underlines the non-predictability of assembly processes.[35,36]

Single- ***versus*** **double-stranded 1D-coordination polymer with ligand 2**

Red single crystals grown from a MeOH solution of $Zn(OAc)_2$·2H_2O layered over a $CHCl_3$ solution of **2** proved to be the 1D-coordination polymer [{$Zn(OAc)_2$(**2**)}·MeOH·H_2O]$_n$. The compound crystallizes in the orthorhombic space group *Pbca*, with polymer chains propagating along the crystallographic *a*-axis. Fig. 5 depicts the repeat unit with symmetry-generated atoms. Each of the two crystallographically independent Zn atoms is coordinated by the N atom of two different 4,2':6',4''-tpy units and by two monodentate acetato ligands; the acetate group with O4 shows a weak second contact to Zn1 (Zn1–O4 = 2.751(2) Å). Bond distances in the coordination sphere (caption to Fig. 5) are typical with N–Zn–O, N–Zn–N and O–Zn–O bond angles in the range 98.67(9) to 121.23(9)°. Each ferrocenyl group has an eclipsed conformation, and each C_5H_4-ring is close to coplanar with the pyridine ring to which it is bonded. As in [{ZnI_2(**2**)}$_4$·1.4MeOH·0.8H_2O], this is attributed to packing effects (see below). The 1D-chain in [{$Zn(OAc)_2$(**2**)}·MeOH·H_2O]$_n$ is similar to that reported for [{$Zn(OAc)_2$(**2**)}·2H_2O]$_n$ (CSD refcode TUNCIQ[21]) and an overlay of the two structures is shown in Fig. 6. In [{$Zn(OAc)_2$(**2**)}·MeOH·H_2O]$_n$, the chain is built up by translation (space group *Pbca*), whereas in [{$Zn(OAc)_2$(**2**)}·2H_2O]$_n$ (space group $P2_1/n$) the chain is built up by a glide plane; these assemblies are similar to those of [ZnX_2(4'-(4-(3-chloropyridyl))-4,2':6',4''-tpy)]$_n$ (X = Cl, I)[36] and [ZnI_2(4'-(4-pyridyl)-4,2':6',4''-tpy)]$_n$[37] and stand apart from the range of helical [ZnY_2(4'-R-4,2':6',4''-tpy)]$_n$ chains (R and Y = various) built up along screw axes.[22]

Adjacent chains in [{Zn(OAc)$_2$(**2**)}·MeOH·H$_2$O]$_n$ interact through π-stacking of pairs of pyridine and cyclopentadienyl rings (Fig. 7). Both independent Cp$_2$Fe units are involved, and the distances from the centroid of the C$_5$H$_4$ ring containing C11 or C36 (see Fig. 5) to the plane of the pyridine ring containing N4^{iii} or N1^{iv} (symmetry codes iii = $-x$, $-{}^1/_2+y$, ${}^1/_2-z$, iv = $-x$, ${}^1/_2+y$, ${}^1/_2-z$) are 3.35 and 3.29 Å, respectively.

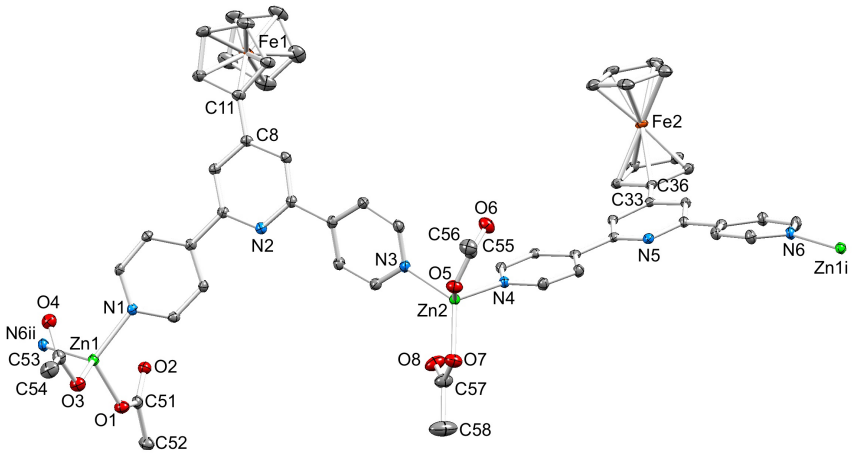

Fig. 5. Structure of the repeat unit in [{Zn(OAc)$_2$(**2**)}·MeOH·H$_2$O]$_n$ with symmetry-generated atoms; H atoms and solvent molecules are omitted and ellipsoids plotted at 30% probability level. Symmetry code i = $-1+x$, y, z, ii = $1+x$, y, z. Selected bond distances: Zn1–N6^{ii} = 2.033(2), Zn1–N1 = 2.030(2), Zn1–O1 = 1.9403(19), Zn1–O3 = 1.955(2), Zn2–N3 = 2.036(2), Zn2–N4 = 2.028(2), Zn2–O5 = 1.936(2), Zn2–O7 = 1.947(2) Å.

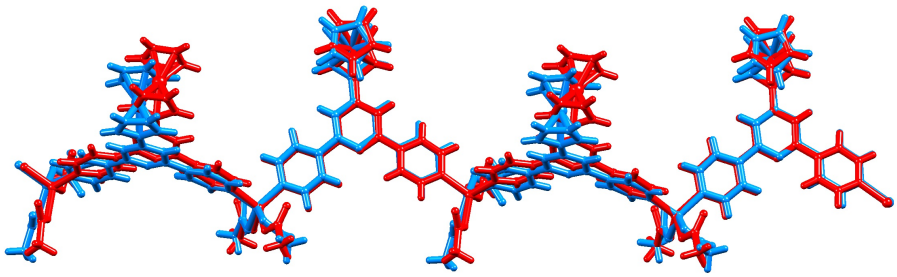

Fig. 6. Overlay of parts of the 1D-coordination polymer chains in [{Zn(OAc)$_2$(**2**)}·MeOH·H$_2$O]$_n$ (red) and [{Zn(OAc)$_2$(**2**)}·2H$_2$O]$_n$ (blue, CSD refcode TUNCIQ).

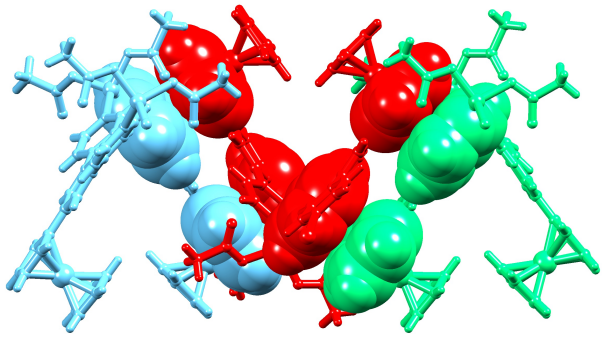

Fig. 7. Three adjacent chains in [{$Zn(OAc)_2$(**2**)}·MeOH·H_2O]$_n$ viewed down the *a*-axis; solvent molecules are omitted. Pyridine...cyclopentadienyl π-stacking interactions are shown in spacefilling representation.

Coordination assemblies formed between zinc(II) salts and 4,2':6',4''-tpy ligands are typified by 2-connecting zinc nodes, compatible with either 1D-coordination polymers or metallomacrocycles. We argued that a change from $ZnCl_2$ to $CuCl_2$ should introduce the potential for increased coordination number at the metal node as well as chlorido-bridge formation. Red plates grew over a period of several days when a MeOH/$CuCl_2$ solution was layered over a $CHCl_3$/**2** solution at room temperature. Single crystal X-ray diffraction revealed the formation of the coordination polymer [{Cu_2Cl_4(**2**)$_2$(MeOH)}·2.25MeOH·H_2O·$CHCl_3$]$_n$; SQUEEZE[28] was used to treat part of the solvent region. The repeat unit of the polymer is shown in Fig. 8, and selected bond lengths are given in the figure caption. The chain is supported by a {Cu_2Cl_2(μ-Cl)$_2$} unit; this building block is well represented in the Cambridge Structural Database[34] (402 hits found in the CSD v. 5.37 with updates to Feb 2016, using Conquest v. 1.18[26]). Each Cu atom binds two *N*-donor atoms of two different 4,2':6',4''-tpy units in a *trans*-arrangement leading to the assembly of a double-stranded chain (Fig. 9a). This type of assembly has previously been observed with {$Cd_2(OAc)_4$} nodes connecting 4'-(4-biphenylyl)-4,2':6',4''-tpy linkers,[18] and related nodes in [Cd(1,4-ndc)(4'-(4-pyridyl)- 4,2':6',4''-tpy)·1.5H_2O]$_n$ (H_2ndc = 1,4-naphthalene dicarboxylic acid) direct a 3D-'pillar-layer' assembly which incorporates double-stranded chains.[38] A MeOH molecule completes the octahedral coordination sphere of atom Cu1 (Fig. 8), whereas Cu2 is 5-coordinate (square-based pyramidal). There are no short contacts within the lattice to fill the vacant coordination site.[39]

Each of the two crystallographically independent tpy units is close to planar and the C_5H_4 ring of each ferrocene substituent is twisted only 6.2° out of the plane of the pyridine ring to which it is attached. Once again, this is a consequence of π-stacking contacts and Fig. 9b shows how this extends along the length of the chain, and that the pairs of heterocyclic rings adopt an optimal offset arrangement. The separation of stacked pairs of 4,2':6',4''-tpy units (~3.4 Å) is slightly shorter than the Cu...Cu distance in each $\{Cu_2Cl_4\}$ node (Cu...Cu = 3.667(1) Å). Fig. 9b also shows that pairs of Cp_2Fe groups containing Fe1/Fe2^{i} and Fe2/Fe1^{i} (symmetry code i = $^1/_2-x$, $-^1/_2+y$, $^1/_2-z$) also stack across the double-stranded chain (angle between Cp planes = 5.5°; intercentroid distance = 3.81 Å).

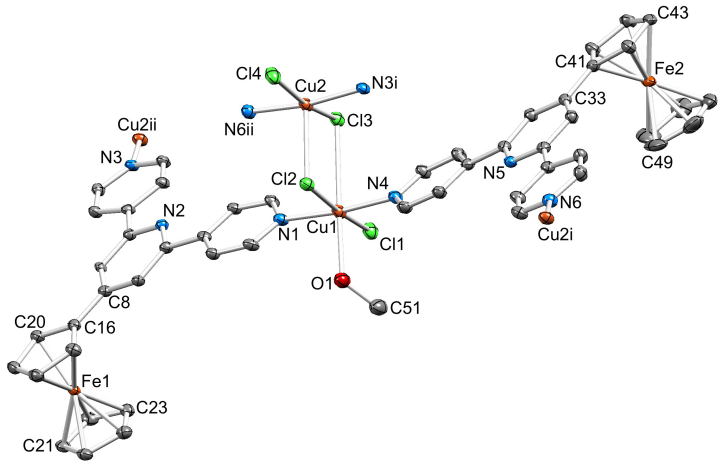

Fig. 8. Structure of the repeat unit in $[\{Cu_2Cl_4(\mathbf{2})_2(MeOH)\}\cdot 2.25MeOH\cdot H_2O\cdot CHCl_3]_n$ with symmetry-generated atoms; H atoms and solvent molecules are omitted and ellipsoids plotted at 30% probability level. Symmetry code i = $^1/_2-x$, $-^1/_2+y$, $^1/_2-z$, ii = $^1/_2-x$, $^1/_2+y$, $^1/_2-z$. Selected bond distances: Cu1–Cl1 = 2.3406(15), Cu1–Cl2 = 2.3688(14), Cu1–Cl3 = 3.0436(14), Cu1–N1 = 1.996(4), Cu1–N4 = 1.992(4), Cu1–O1 = 2.319(4), Cu2–N6^{ii} = 2.001(4), Cu2–N3^{i} = 2.000(4), Cu2–Cl2 = 2.6392(13), Cu2–Cl3 = 2.3008(14), Cu2–Cl4 = 2.3333(16) Å.

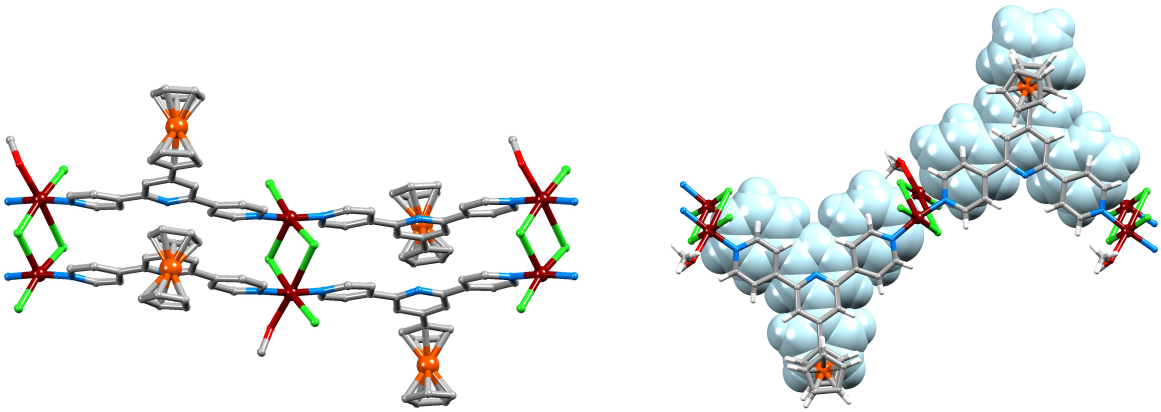

(a) (b)

Fig. 9. (a) Part of one double-stranded chain in [{Cu_2Cl_4(**2**)$_2$(MeOH)}·2.25MeOH·H_2O·$CHCl_3$]$_n$ (viewed down the *a*-axis) and (b) the same chain viewed down the *c*-axis to show the face-to-face π-stacking; the back chain is shown in spacefilling representation.

From a 4,2':6',4''- to 3,2':6',3''-tpy donor set

While the directionality of the *N,N''*–donor set in 4,2':6',4''-tpy is fixed, that in 3,2':6',3''-tpy varies as the interannular C–C bonds rotate.[31] Thus, the change in the vectorial properties of the *N*-donor set on going from **2** to **3** (Scheme 2) reduces (still further) the predictability of the metal-binding mode. Methanol solutions of $ZnCl_2$ or $ZnBr_2$ were layered over chloroform solutions of **3**, and red blocks grew in both crystallization tubes within two weeks. Single crystal X-ray diffraction showed the products to be the discrete molecule [{$ZnCl_2$(**3**)}$_4$·3$CHCl_3$·3MeOH] and the 1D-coordination polymer [{$ZnBr_2$(**3**)}·MeOH]$_n$, respectively.

[{$ZnCl_2$(**3**)}$_4$·3$CHCl_3$·3MeOH] crystallizes in the orthorhombic space group *Pccn* with half of the molecule in the asymmetric unit. The second half is generated by a 2-fold axis, and Fig. 10 depicts the resulting metallosquare. Each Zn atom is tetrahedrally sited with typical Zn–N and Zn–Cl distances (caption to Fig. 10); the bond angles in the coordination spheres of Zn1 and Zn2 range from 98.1(3) to 117.5(2)°. The 3,2':6',3''-tpy unit in each coordinated **3** adopts a *cis*,*trans*-conformation (Fig. 10), with angles between the planes of the rings containing N1/N2, N2/N3 and N4/N5, N5/N6 being 17.9, 23.2° and 37.7, 17.8°. Each of the two independent ferrocenyl units has an eclipsed conformation and the plane of the C_5H_4 ring is twisted (12.6 and 14.4°, respectively) with respect to the central pyridine ring of each 3,2':6',3''-tpy unit. Although these twist angles are similar, only one is associated with a C_5H_4...pyridine π-

stacking contact. The cyclopentadienyl ring containing C36 lies in an offset orientation over the ring containing N1^{ii} (symmetry code iii = $^{1}/_{2}+x$, $1-y$, $^{1}/_{2}-z$) with centroid...centroid separation of 3.51 Å; the angle between the ring planes is 3.6° and the pyridine(plane)...C_6H_4(centroid) distance is 3.29 Å. When viewed down the crystallographic *a*-axis, the {$ZnCl_2$(**3**)}$_4$ tetramer adopts a V-shaped conformation and molecules pack along the *b*-axis with π-stacking interactions between the pyridine rings[40] containing N2 and N5^{iii} (symmetry code iii = $1-x$, $-^{1}/_{2}+y$, $^{1}/_{2}-z$) as shown in Fig. 11. The interaction between offset (but mutually twisted) rings are characterized by the distances ring N2-centroid...ring N5^{iii}-plane = 3.58 Å, centroid...centroid separation = 3.72 Å, and an angle between the pyridine ring planes of 2.9°. The V-shaped cavity of {$ZnCl_2$(**3**)}$_4$ hosts at least one $CHCl_3$ molecule, but we refrain from a discussion of molecule...solvent interactions because some solvent molecules were removed by SQUEEZE (see experimental section). In contrast to the situation for [{ZnI_2(**2**)}$_4$·1.4MeOH·0.8H_2O] (see earlier), we were unable to confirm if the metallosquare in [{$ZnCl_2$(**3**)}$_4$·3$CHCl_3$·3MeOH] is representative of the bulk sample; only a few single crystals were obtained and the bulk material was an amorphous powder unsuited to powder X-ray diffraction. However, competitive assembly processes are indicated by a report[41] of the 1D-coordination polymer [{$ZnCl_2$(**3**)}·1.5H_2O]$_n$ but no details of synthesis are available.

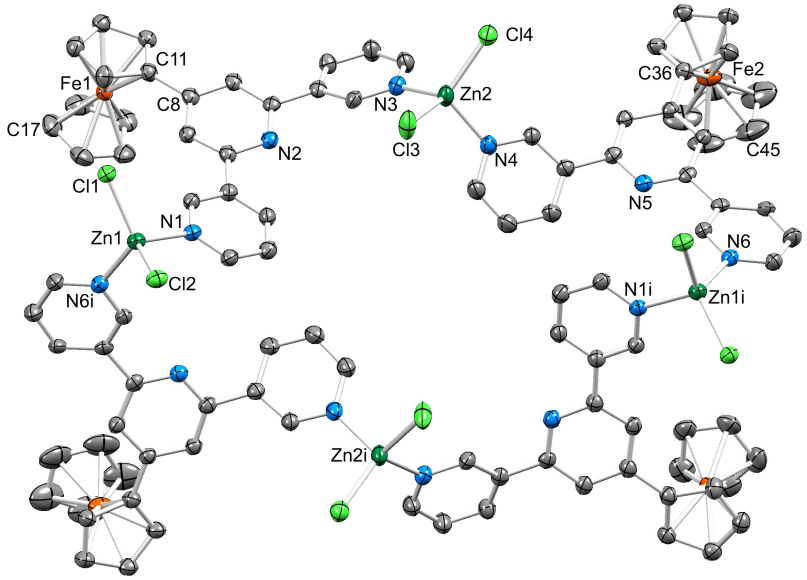

Fig. 10. Structure of the {$ZnCl_2$(**3**)}$_4$ molecule in [{$ZnCl_2$(**3**)}$_4$·3$CHCl_3$·3MeOH]; H atoms and solvent molecules are omitted and ellipsoids plotted at 30% probability level. Symmetry code i = $^{1}/_{2}-x$, $^{1}/_{2}-y$, z. Selected bond distances: Zn1–N6^{i} = 2.063(8), Zn1–Cl1 = 2.202(2), Zn1–Cl2 = 2.235(3), Zn1–N1 = 2.074(8), Zn2–Cl3 = 2.243(3), Zn2–Cl4 = 2.224(3), Zn2–N3 = 2.043(8), Zn2–N4 = 2.038(9) Å.

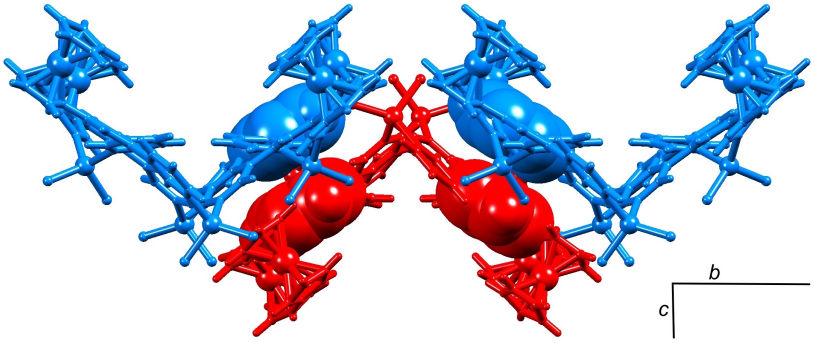

Fig. 11. Adjacent metallosquares in [{$ZnCl_2$(**3**)}$_4$·3$CHCl_3$·3MeOH] interact along the *b*-axis through π-stacking interactions between pairs of pyridine rings.

The repeat unit in the 1D-coordination polymer [{$ZnBr_2$(**3**)}·MeOH]$_n$ (which crystallizes in the triclinic space group *P*–1) is depicted in Fig. 12. Both independent Zn atoms are tetrahedrally coordinated; bond distances are in the caption to Fig. 12, and bond angles lie between 96.54(12)° (N3–Zn2–N4) and 119.17(2)° (Br3–Zn2–Br4). As in the other structures in this work, the ferrocene units are in eclipsed conformations. The functionalized C_5 ring of one unit (with Fe1) lies only 6.4° out of the plane of the pyridine ring to which it is bonded, while the second is significantly twisted (41.3°, see later). The 3,2':6',3''-tpy unit containing N1, N2 and N3 is in a *cis,cis*-conformation, with pairs of rings with N1/N2 and N2/N3 mutually twisted through 7.8 and 35.7°, respectively. In contrast, the ligand with N4, N5 and N6 adopts a *cis,trans*-conformation, and adjacent rings are twisted through 24.8 and 25.0°. These differences in conformation lead to alternating short and long Zn...Zn separations (Zn1...Zn2 = 6.7181(7) Å and Zn2...Zn1^{i} = 11.0715(9) Å). The 1D-chain is built up by translation, but the helical twist within the asymmetric unit (Fig. 12) leads to a chiral polymer; chains of both handednesses are present in the unit cell. The helical chain has a pitch of 8.7879(9) Å (Zn1...Zn1^{i}). This tight turn is related both to the orientations of the *N,N*''-donor sets in the 3,2':6',3''-tpy units, and to the π-stacking interactions within the chain (Fig. 13). The latter occur between the Cp ring containing C16 and the two pyridine rings with N1^{iii} and N2^{iii} (symmetry code iii = 1+*x*, *y*, *z*). The distance from the least squares plane through the two pyridine rings and the centroid of the Cp ring is 3.42 Å, and the angle between the planes through the stacked units is 8.3°. An analogous packing motif is present in [{$ZnCl_2$(**3**)}·1.5H_2O]$_n$, but this structure has not been discussed in detail.[41]

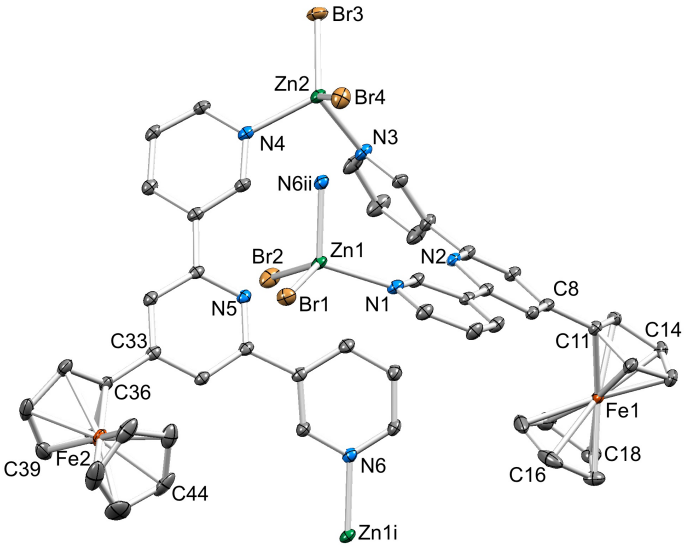

Fig. 12. Structure of the repeat unit in $[\{ZnBr_2(\mathbf{3})\}\cdot MeOH]_n$ with symmetry-generated atoms; ellipsoids are plotted at 30% probability level, and H atoms and solvent molecules are omitted. Symmetry code i = 1–*x*, *y*, *z*, ii = –1+*x*, *y*, *z*. Selected bond distances: Zn1–N6^{ii} = 2.038(3), Zn1–Br1 = 2.3504(6), Zn1–Br2 = 2.3587(6), Zn1–N1 = 2.041(3), Zn2–Br3 = 2.3515(6), Zn2–Br4 = 2.3455(6), Zn2–N3 = 2.050(3), Zn2–N4 = 2.059(3) Å.

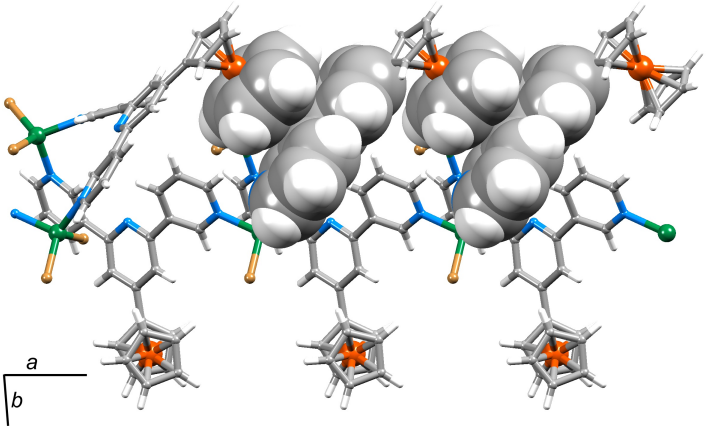

Fig. 13. Part of one helical chain in $[\{ZnBr_2(\mathbf{3})\}\cdot MeOH]_n$ (solvent molecules are omitted) which follows the *a*-axis. Intra-chain π-stacking interactions (see text) are shown in space-filling representation.

Conclusions

The synthesis and characterization, including a single crystal structure determination, of ligand **3** have been described. Both **2** and **3** coordinate metal ions through the outer two pyridine rings. Reactions of **2** with $ZnCl_2$ and $ZnBr_2$ lead to discrete metallohexacycles which confirms earlier an report.[21] However,

predictable assembly algorithms cannot be assumed as demonstrated by the formation of either a 1D-polymer[21] or a discrete metallosquare (this work) when ZnI_2 reacts with **2** apparently under the same conditions of crystal growth. A switch from single- to double-stranded 1D-polymer chains is achieved by combining the divergent donor set of **2** with $Zn(OAc)_2$ or $CuCl_2$; the potential for increased coordination number of Cu(II) versus Zn(II) and the propensity for formation of bridging chlorido ligands leads to dinuclear metal nodes which support a double-stranded chain. Whereas **2** exhibits a fixed V-shaped donor set, its isomer **3** offers greater variation in the vectorial properties of the donor set. This has been demonstrated in the reactions of **3** with $ZnCl_2$ or $ZnBr_2$ which lead, respectively, to a metallosquare in $[\{ZnCl_2(\mathbf{3})\}_4 \cdot 3CHCl_3 \cdot 3MeOH]$ but to a helical polymer in $[\{ZnBr_2(\mathbf{3})\} \cdot MeOH]_n$. The tight pitch of the helix in the latter (8.7879(9) Å) is governed by a combination of the orientations of the *N,N''*-donor sets in the 3,2':6',3''-tpy units in **3**, and to intra-chain π-stacking interactions involving ferrocenyl and pyridine units.

Although the 4,2':6',4''-tpy unit in **2** offers a fixed V-shaped donor set, it does not lead to a predictable assembly algorithm; under similar crystal growth conditions, polymer and metalloamacrocycle formation (both 4- and 6-membered rings) may be in competition. Similar competitive behaviour is observed for ligand **3** with zinc(II) halides, but the greater conformational flexibility of **3** versus **2** adds to the non-predictability of the outcome of the assembly process.

Acknowledgements

We thank the Swiss National Science Foundation (Grant number 200020_144500) and the University of Basel for support. The Swiss National Science Foundation through the NCCR Molecular Systems Engineering is acknowledged for partial funding of the powder diffractometer.

References

[1] R. Horikoshi, *Coord. Chem. Rev.* **2013**, *257*, 621. doi:10.1016/j.ccr.2012.09.026

[2] O. Oms, J. Le Bideau, F. Leroux, A. van der Lee, D. Leclercq, A. Vioux, *J. Am. Chem. Soc.* **2004**, *126*, 12090. doi:10.1021/ja049457p

[3] J. G. Eaves, R. Mirrazaei, D. Parker, H. S. Munro, *J. Chem. Soc., Perkin Trans. 2* **1989**, 373. doi:10.1039/P29890000373.

[4] B. Adhikari, C. Singh, A. Shah, A. J. Lough, H.-B. Kraatz, *Chem. Eur. J.* **2015**, *21*, 11560. doi:10.1002/chem.201501395

[5] M. Kubo, Y. Mori, M. Otani, M. Murakami, Y. Ishibashi, M. Yasuda, K. Hosomizu, H. Miyasaka, H. Imahori, S. Nakashima, *J. Phys. Chem. A* **2007**, *111*, 5136. doi: 10.1021/jp071546b

[6] C. Bucher, C. H. Devillers, J.-C. Moutet, G. Royal, E. Saint-Aman, *Chem. Commun*. **2003**, 888. doi:10.1039/B301177A

[7] M. C. Carrión, F. A. Jalón, A. López-Agenjo, B. R. Manzano, W. Weissensteiner, K. Mereiter, *J. Organomet. Chem.* **2006**, *691*, 1369. doi:10.1016/j.jorganchem.2005.12.023

[8] H.-U. Blaser, W. Brieden, B. Pugin, F. Spindler, M. Studer, A. Togni, *Top. Catal.* **2002**, *19*, 3. doi:10.1023/A:1013832630565

[9] O. Carugo, G. De Santis, L. Fabbrizzi, M. Licchelli, A. Monichino, P. Pallavicini, *Inorg. Chem.* **1992**, *31*, 765. doi:10.1021/ic00031a014

[10] T. Mochida, F. Shimizu, H. Shimizu, K. Okazawa, F. Sato, D. Kuwahara, *J. Organomet. Chem.* **2007**, *692*, 1834. doi: 0.1016/j.jorganchem.2006.11.011

[11] R. Horikoshi and T. Mochida, *Eur. J. Inorg. Chem.* **2010**, 5355. DOI: 10.1002/ejic.201000525

[12] D. Braga, M. Polito, M. Bracaccini, D. D'Addario, E. Tagliavini, D. M. Proserpio, F. Grepioni, *Chem. Commun.* **2002**, 1080. doi:10.1039/B200344A

[13] N. Sadhukhan, J. K. Bera, *Inorg. Chem.* **2009**, *48*, 978. doi:10.1021/ic801586d

[14] D. Braga, M. Curzi, S.L. Giaffreda, F. Grepioni, L. Maini, A. Pettersen, M. Polito in 'Ferrocenes: Ligands, materials and biomolecules', ed. P. Stepnicka, **2008**, Wiley, Chichester.

[15] See for example: P. Lai-Tee, T. S. A. Hor, Z. Zhong-Yuan, T. C. W. Mak, *J. Organomet. Chem.* **1994**, *469*, 253. doi:10.1016/0022-328X(94)88080-8

[16] M. Concepcion Gimeno, P. G. Jones, A. Laguna, C. Sarroca, *J. Chem. Soc., Dalton Trans.* **1998**, 1277. doi:10.1039/A708959G

[17] Y. M. Klein, A. Prescimone, E. C. Constable, C. E. Housecroft, *Inorg. Chem. Commun.* **2016**, *70*, 118. doi:10.1016/j.inoche.2016.05.027

[18] E. C. Constable, C. E. Housecroft, M. Neuburger, J. Schönle, S. Vujovic, J. A. Zampese, *Polyhedron* **2013**, *60*, 120. doi:10.1016/j.poly.2013.05.026

[19] E. C. Constable, G. Zhang, E. Coronado, C. E. Housecroft, M. Neuburger, *CrystEngComm* **2010**, *12*, 2139. doi:10.1039/B926597J

[20] E. C. Constable, C. E. Housecroft, S. Vujovic, J. A. Zampese, A. Crochet and S. R. Batten, *CrystEngComm* **2013**, *15*, 10068. DOI: 10.1039/C3CE41384E

[21] L. Xiao, L. Zhu, Q. Zeng, Q. Liu, J. Zhang, S. Li, H. Zhou, S. Zhang, J. Wu, Y. Tian, *J. Organomet. Chem.* **2015**, *789–790*, 22. doi:10.1016/j.jorganchem.2015.05.007

[22] C. E. Housecroft, *Dalton Trans.* **2014**, *43*, 6594. doi: 10.1039/C4DT00074A and references therein.

[23] Bruker Analytical X-ray Systems, Inc., 2006, APEX2, version 2 User Manual, M86-E01078, Madison, WI.

[24] L. Palatinus, G. Chapuis, *J. Appl. Cryst.* **2007**, *40*, 786. doi: 10.1107/S0021889807029238

[25] P. W. Betteridge, J. R. Carruthers, R. I. Cooper, K. Prout, D. J. Watkin, *J. Appl. Cryst*. **2003**, *36*, 1487. doi: 10.1107/S0021889803021800

[26] I. J. Bruno, J. C. Cole, P. R. Edgington, M. K. Kessler, C. F. Macrae, P. McCabe, J. Pearson and R. Taylor, *Acta Cryst. B* **2002**, *58*, 389. doi: 10.1107/S0108768102003324.

[27] C. F. Macrae, I. J. Bruno, J. A. Chisholm, P. R. Edgington, P. McCabe, E. Pidcock, L. Rodriguez-Monge, R. Taylor, J. van de Streek and P. A. Wood, *J. Appl. Cryst.* **2008**, *41*, 466. doi: 10.1107/S0021889807067908

[28] A. L. Spek, *Acta Crystallogr., Sect. C* **2015**, *71*, 9. doi:10.1107/S2053229614024929

[29] I.R. Butler, S.J. McDonald, M.B. Hursthouse and K.M.A. Malik, *Polyhedron*, 1995, **14**, 529. doi: 10.1016/0277-5387(94)00266-H.

[30] T.M. Miller, K.J. Ahmed and M.S. Wrighton, *Inorg. Chem*. **1989**, *28*, 2347. DOI: 10.1021/ic00311a020.

[31] C. E. Housecroft, *CrystEngComm* **2015**, *17*, 7461. doi: 10.1039/C5CE01364J.

[32] Y.M. Klein, A. Prescimone, E. C. Constable, C. E. Housecroft, unpublished results.

[33] E. C. Constable, C. E. Housecroft, A. Prescimone, S.Vujovic and J. A. Zampese *CrystEngComm* **2014**, *16*, 8691. doi: 10.1039/c4ce00783b.

[34] C.R. Groom, I.J. Bruno, M.P. Lightfoot, S. C. Ward, *Acta Cryst*. **2016**, *B72*, 171. doi

10.1107/S2052520616003954.

[35] E.C. Constable, C.E. Housecroft, B.M. Kariuki, N.Kelly, C.B. Smith, *Comptes Rendues* **2002**, *5*, 425. doi.org/10.1016/S1631-0748(02)01401-7

[36] E.C. Constable, G. Zhang, C.E. Housecroft, J. A. Zampese, *CrystEngComm* **2011**, *13*, 6864. DOI: 10.1039/C1CE05884C.

[37] J. Heine, J. S. auf der Gunne, S. Dehnen, *J. Am. Chem. Soc.* **2011**, *133*, 10018. DOI: 10.1021/ja2030273.

[38] D.L. An, Y-Q. Chen, Y. Tian, *Z. Anorg. Allg. Chem.* **2014**, *640*, 1776. DOI: 10.1002/zaac.201400037

[39] E. C. Constable, C. E. Housecroft, J. R. Price, J. A. Zampese, *CrystEngComm* **2010**, *12*, 3163. DOI: 10.1039/C0CE00019A

[40] C. Janiak, *CrystEngComm* **2000**, 3885. doi. 10.1039/B003010O.

[41] L. Xiao, Y. Tian, **2015**, private communication to the CSD, refcode VUKMOF.